Full Modeling, Loss Reduction, and Mutual Coupling Control of Spoof Surface Plasmon-Based Meander Slow Wave Transmission Lines

Amin Kianinejad, *Member, IEEE*, Zhi Ning Chen, *Fellow, IEEE,* and Cheng-Wei Qiu, *Member, IEEE*

***Abstract*—The full models of meander spoof surface plasmon (SSP) cells are presented for the design of slow wave transmission lines (SW-TLs) with the minimum loss and controllable mutual coupling (MC). In addition to the modeling of dispersion curve and characteristic impedance, the proposed circuit model based on geometrical parameters calculates the ohmic loss of the SW-TLs composed of meander SSP cells. Being verified with the full-wave analysis, the model provides a clear understanding of the mechanism of the SSP-based SW-TLs and a new way to design with other circuits at a system level. The model is applied to minimize the ohmic loss in the meander SW-TLs up to at least 10 dB per 10 wavelengths lower than that of conventional TLs. The MC of the SW-TLs can be controlled either up to three orders of magnitude lower or one order of magnitude higher than that of the conventional TLs. This paper proposes methods to decrease the ohmic loss of single-layered meander SW-TLs and also controls MC between them. The proposed methods open new avenues for complex and compact circuit designs.**

***Index Terms*—Compact circuit modeling, crosstalk, impedance matching, periodic structures, plasmons, transmission line (TL) transition.**

I. Introduction

SPOOF surface plasmon (SSP) modes are highly localized surface waves mimicking the characteristics of real optical surface plasmon polariton modes [1] and are ranging from subgigahertz [2] to terahertz regime [3], [4]. Shen *et. al.* [5] proposed an ultrathin planar corrugated metal strip supporting SSP modes.

Conversion of confined SSP modes to radiating modes was studied in [6]–[12]. In [8], an SSP-based waveguide feeds an array of microstrip patch antennas. Another study applied SSP-based waveguides to control the radiation from dielectric slabs [9]. Wu *et. al.* [10] studied the leaky-wave radiation from the SSP modes. Leaky-wave antennas with single-layer configurations based on SSP modes were also proposed in [12] and [13].

In fact, Goubau [14] first introduced the concept of "single wire" transmission line (TL) which was a metal wire coated with dielectric. Goubau line was then developed in later works [15]–[17]. Recently, several efficient transitions have been introduced to connect single-layered SSP structures to microstrip TLs and coplanar waveguides (CPWs) [18], [19]. SSPs have been applied to design microwave components such as frequency splitters [20], filters [21]–[26], couplers [27], and multiband TLs [28]. SSP mode-based-TLs have also found their ways into on-chip CMOS designs [29]. The ohmic loss in spoof plasmon TLs has been studied widely in the literature [19], [29]–[31]. Zhang *el. al.* [30] showed that comb-shaped structures have a lower ohmic loss in comparison with conventional TLs. Despite the number of works on SSP loss, a reliable model for this important parameter is still needed for further SSP-based design purposes.

Meander lines have been applied in electromagnetic (EM) structures. A circuit model is developed for meander-line networks and formation of circular polarizers [32], [33]. Meander SSP structures were studied in [34]. A recent work [11] has shown that single-layered meander structures support SSP modes. These structures are also beneficial to excite the TE modes of dielectric resonator antennas [11] as well as to form wideband leaky-wave antennas [12].

The U-shaped and H-shaped SSP cells were modeled with circuit elements in [19] and [35]. The EM fields are distributed only over one side of single-sided U-shaped SSP cells. On the other hands, H-shaped cells benefit from their double-sided structures and are more compatible with conventional TLs; however, their profiles are two times as wide as U-shaped cells at the identical frequency range. In contrast, meander SSP cells with their double-sided configuration provide high compatibility with conventional TLs while benefiting from their low-profile configuration as wide as single-sided U-shaped SSP cells.

The meander SSP cells need reliable and repeatable circuit model in order to further promote their implementation and enhance their compatibility with other circuit elements. This paper extends the previous geometry-based modeling of SSP structures to the meander cells and further develops the model by incorporating the ohmic loss for the very first time using a parallel conductance to provide a full modeling. Being verified by simulations and experiments, the model is applied to minimize the ohmic loss of meander-line slow wave TLs (SW-TLs).

On the other hand, one of the major challenges for miniaturization of the integrated circuits is the mutual coupling (MC) of the circuit components and to acquire highly compact

Manuscript received August 29, 2017; revised November 18, 2017 and March 7, 2018; accepted April 17, 2018. Date of publication June 8, 2018; date of current version August 6, 2018. *(Corresponding author: Amin Kianinejad.)*

The authors are with the Department of Electrical and Computer Engineering, National University of Singapore, Singapore 117583 (e-mail: amin@u.nus.edu; eleczn@nus.edu.sg; chengwei.qiu@nus.edu.sg).

Color versions of one or more of the figures in this paper are available online at http://ieeexplore.ieee.org.

Digital Object Identifier 10.1109/TMTT.2018.2841857

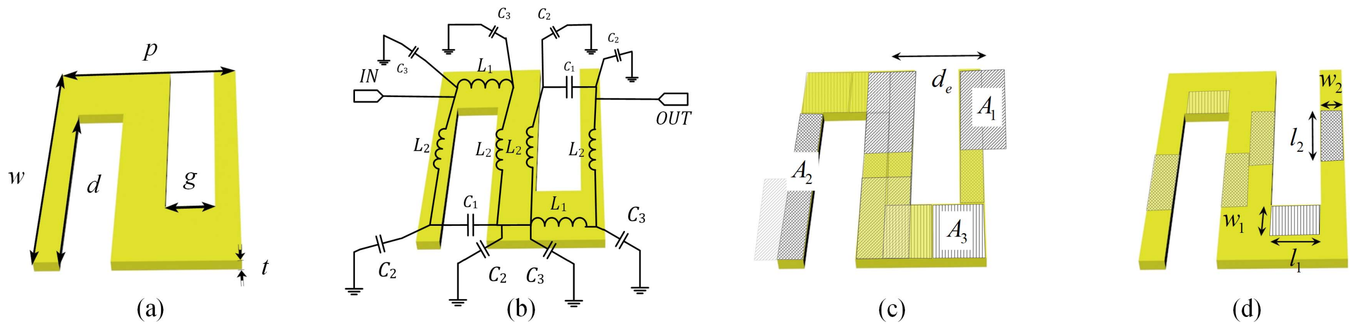

Fig. 1. (a) One unit cell of meander SSP. (b) Equivalent circuit model. (c) Effective areas for equivalent capacitors. (d) Effective areas of current paths for equivalent inductors.

circuits, it is required to minimize the MC effects between the elements to suppress any possible interference. In contrast, highly coupled TLs are also required in circuits, for example, couplers. Consequently, the possibility of MC control is an advantageous feature for TLs.

Wu *et al.* [36] added corrugation to microstrip TLs to reduce the MC between the TLs. Liang *et al.* [37], [38] studied the MC between the U-shaped SW-TLs with a coplanar back-to-back configuration in subterahertz in CMOS. In [39], the double-layered corrugated strips supporting time-domain SSPs were applied to significantly decrease the crosstalk between TLs. In [35], the MC and loss of H-shaped SW-TLs were investigated.

The MC between the conventional TLs is determined by the configuration of two closely located lines and cannot be changed within a fixed arrangement. The SSP cells of SW-TLs with their controllable geometries, on the other hand, provide extra degrees of freedom to control the MC within a fixed configuration. The presented work first demonstrates this feature of SW-TLs and evidences the dynamic range of 40-dB MC control for the coupled SW-TLs with the coupled line length of 5λ. A method for the suppression of the MC between SW-TLs is proposed. The presented coupling adjustment method can be applied for suppression of the coupling between any SW-TLs.

Furthermore, the equivalent circuit model for the meander SSP cells is presented and discussed. After that, the ohmic loss in the meander SW-TLs is numerically and experimentally studied and modeled using circuit elements. The MC between the meander SW-TLs is studied as well.

II. Circuit Modeling

A single-layered meander structure as shown in Fig. 1(a) supports SSP modes and acts as a low-profile SSP cell. Similar to U-shaped and H-shaped SSP cells, meander cells need a reliable and repeatable circuit model to increase their compatibilities with other circuit components in circuit designs. One unit cell is depicted in Fig. 1(a) with the following geometrical parameters: the period length of p, width of w, groove width of g, groove depth of d, and thickness of t.

Fig. 1(b) presents the circuit model. The voltage is defined as the voltage difference between the cell and infinity, while the current is defined as the surface current at the SSP cells. The inductors and capacitors model the EM behavior of SSP modes. To model the electric fields inside the gap, the capacitor C_1 connects the two sides of the grooves. To initiate the connection of the cell to a ground plane, the capacitance of the isolated metal is modeled by C_2 and C_3. The equivalent inductors L_1 and L_2 model the surface current at the SSP cells.

In the proposed model, the SSP unit cell is divided into several segments where each segment has an inductive or capacitive response. The model applies the electrostatic approximation to calculate the equivalent inductors and capacitors. This approximation requires knowledge of the surface charge and current distribution over the SSP cell. However, these distributions are not uniform through the cell, and consequently, it is necessary to define the effective areas for the calculation of the equivalent circuit elements. This section defines the effective areas for meander SSP cells with $0.5w < p < 6w$. Fig. 2(c) and (d) depicts the effective metallic plates for capacitors and the current paths for inductors, respectively. As it can be seen, C_1 includes parts of the neighbor periods. The dimensions of the effective current paths in Fig. 1(d) are as follows: $l_1 = g$, $l_2 = h/3$, and $w_2 = (p - 2 \times g)/4$. To minimize the effect of geometry change on the modeling accuracy, two different geometry ranges are defined for w_1. For the meander SSP cells with $0.7w < d$, $w_1 = (w-d)/2$ and for the meander SSP cells with $0.7w > d$, $w_1 = (w-d)/4$. The capacitors are modeled using electrostatic calculation in the CST EM Studio. The inductors are calculated using electrostatic approximation given in [40].

To validate the equivalent circuit, SSP cells of various widths and period lengths are modeled, and the dispersion curves are compared with the results from full-wave analysis. The transient solver of CST Microwave Studio is applied for the full-wave solution of the periodic structure with waveguide ports defined as the excitation sources. The electric fields are observed at different frequencies. Fourier transform over space is applied to the field at each frequency, the maximum result value is located and the wavenumber of the SSP mode is extracted. The procedure is repeated for the monitored fields at all the frequencies.

Fig. 2(a) compares the results for varying cell widths (w). The other parameters of the cells are as follows: $p = 3$ mm, $d = 0.85w$, and $g = 0.25p$. Fig. 2(b) compares the results for varying cell period lengths (p). The other parameters are as follows: $w = 2.3$ mm, $d = 0.85w$, and $g = 0.25p$.

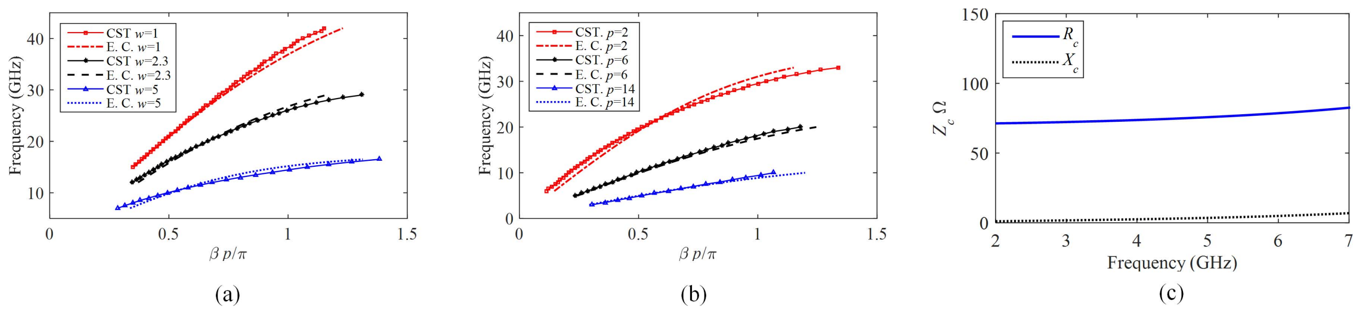

Fig. 2. Comparison between dispersion results of SSP modes in meander cells from equivalent circuit model and full-wave analysis for varying (a) cell widths and (b) cell period lengths. (c) Characteristic impedance of meander SSP cell.

TABLE I

CIRCUIT ELEMENT VALUES FOR MEANDER SSP CELLS

w (mm)	1	2.3	5	2.3	2.3	2.3
p (mm)	3	3	3	2	6	14
C_1 (fF)	4	9	23	10	9	11
C_2 (fF)	19	29	43	24	41	63
C_3 (fF)	11	17	26	14	24	37
L_1 (nH)	0.5	0.4	0.3	0.2	1	2.9
L_2 (nH)	0.05	0.2	0.7	0.3	0.1	0.03

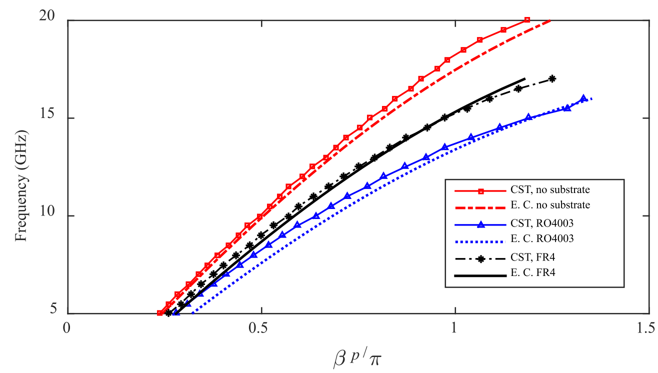

Fig. 3. Effect of dielectric substrate layer on dispersion results.

The comparison validates the model. The values for the equivalent circuit elements of the SSP cells studied in Fig. 2(a) and (b) are tabulated in Table I.

The proposed circuit model is helpful to find the characteristic impedance of the periodic arrangement of SSP cells [41]. Fig. 2(c) plots the real and imaginary parts of impedance for an SSP cell with the following parameters: $p = 4$ mm, $w = 5$ mm, $d = 0.85w$, and $g = 0.25p$. Similar to U-shaped [19] and H-shaped cells [35], the real part is almost constant over the frequency range from 2 to 7 GHz. However, in contrast to the zero imaginary part of the impedance in the two SW-TLs mentioned earlier, the imaginary part X_c for the meander cells is positive showing an inductive characteristic and increases from 0 to 10 Ω over the frequency range of 2–7 GHz.

The equivalent circuit model predicts the effect of dielectric substrate on the dispersion curve. Presence of a dielectric substrate introduces an effective permittivity to the model. An approach similar to [19] and [35] is helpful for calculation of the effective permittivity by comparison of the full-wave analysis results of SSP cells on the substrate layer with that in a uniform medium of the effective permittivity. It is worth mentioning that the presence of the substrate layer only affects the capacitance values. Consequently, the equivalent inductors calculated for SSP cells in free space do not change, while the capacitors are multiplied by the effective permittivity. Fig. 3 compares the dispersion curves of the SSP cells in free space and on pieces of substrate material. Here, Rogers 4003C 0.8 mm and FR4 0.26 mm are considered with the calculated effective permittivity of 1.7 and 1.3, respectively. The SSP cell's parameters are as follows: $p = 6$ mm, $w = 2.3$ mm, $d = 0.85w$, and $g = 0.25p$. Fig. 3 suggests that the agreement between the results and full-wave simulations shows the accuracy of the SSP model on different substrate layers.

To apply the meander cells in microwave circuits and efficiently excite the SSP modes, a compact and high-performance transition to conventional TLs is required. The design procedure for a mode converter for the connection to CPW lines is proposed in [11]. The mode converter is composed of unit cells with the same period length as the TL but with gradually varying width and groove depth. This configuration provides smooth polarization, momentum, and impedance matching simultaneously. A meander SW-TL was designed and fabricated with the following geometrical parameters: $p = 10$ mm, $w = 5$ mm, $d = 3.5$ mm, and $g = 0.25p$ on a piece of Rogers 4003 0.5 mm. The fabricated prototype is depicted in Fig. 4(a). The mode converter is composed of six cells. Fig. 4(b) presents the simulated and measured scattering parameters and indicates the efficient excitation of the SSP modes and desired performance of the SW-TL.

III. LOSS IN SW-TLS

This section examines the different types of losses in meander SW-TLs. Tranmission results from the meander SW-TL as shown in Fig. 4(b) indicate that the total loss in the SW-TL is around 1.2 dB at $2.8\lambda_0$ length of the TL (λ_0 is the wavelength at 7 GHz), which includes all the leaky loss, conversion loss, and ohmic loss.

The leaky loss is the EM wave loss by the undesired radiation from the SSP cells. The generation of the leaky modes by meander SSP cells is studied in [12], where an efficient leaky-wave antenna is designed using meander structures. Here, in order to study the leaky loss, three SW-TLs with varying lengths are compared. To remove the ohmic loss from the calculation, the metal and substrate in SW-TLs are defined as perfect electric conductor and lossless dielectric, respectively.

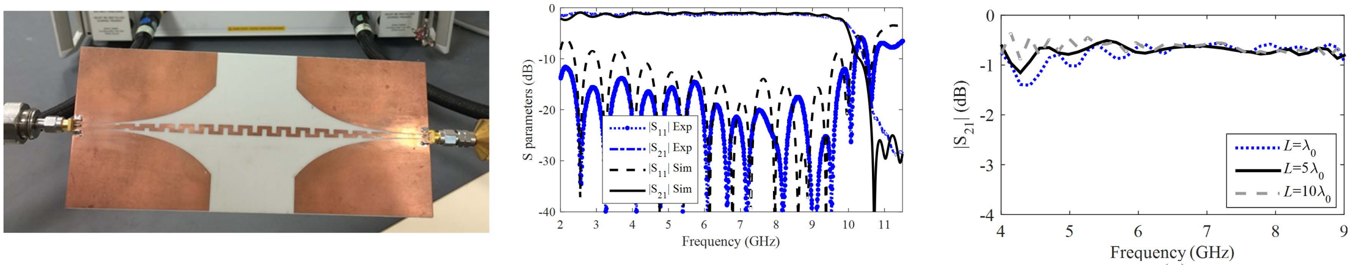

(a) (b) (c)

Fig. 4. (a) Fabricated meander SW-TL. (b) Experimental and simulation scattering parameter results of meander SW-TL. (c) Leaky loss in SW-TLs.

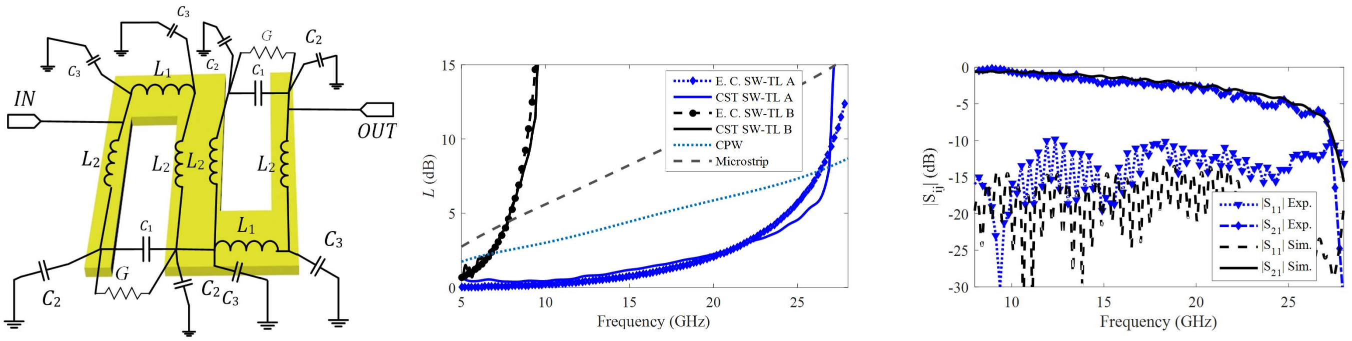

(a) (b) (c)

Fig. 5. (a) Equivalent circuit model of meander SSP cells on lossy dielectric substrate. (b) Comparison between insertion loss of microstrip TL, CPW, and SW-TLs A and B with geometrical parameters given in Table II. (c) Experimental evaluation of SW-TL A.

Fig. 4(c) depicted $|S_{21}|$ for the SW-TLs with three different lengths of λ_0, $5\lambda_0$, and $10\lambda_0$ (λ_0 is the wavelength in free space at 7 GHz). The conversion loss is a fixed value and only caused by the mode converter, while the leaky loss depends on the length of the TL. As it can be seen, by increasing the length, $|S_{21}|$ slightly changes. These results indicate that the constant insertion loss of these SW-TLs with lossless materials is mainly caused by the conversion performance and the leaky loss in the TL is negligible.

The conversion loss is the loss by two-mode converters that connect the meander cells to two CPW lines. For the design in Fig. 4(a), the leaky loss is about 0.4–0.5 dB for each transition. By increasing the number of cells in the converter from 6 to 12, this loss reduces to 0.2 dB.

The ohmic loss in the SW-TL is mainly caused by the imperfect metal and lossy dielectric. The metal loss is modeled by resistors in series with the inductors. The dielectric loss is caused by the current inside the substrate between the edges of the grooves and modeled by the resistors in parallel with the capacitor C_1. Here, the dielectric loss is considered as the main part of the ohmic loss. Fig. 5(a) presents the modified model with additional two resistors in parallel with C_1 modeling the leaky current of this capacitor. The resistor's value is $1/0G$, where G is simply calculated as

$$G = C_1\sigma/\varepsilon_r \tag{1}$$

where ε_r and σ are the dielectric constant and electric conductivity of the substrate, respectively.

In order to suppress the ohmic loss of SW-TL, G should be reduced. According to (1), G is directly proportional

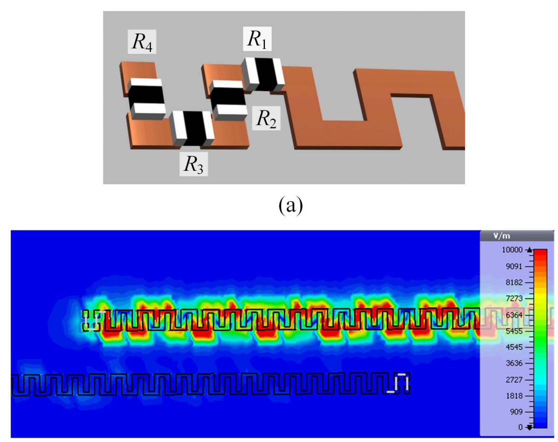

(a)

(b)

Fig. 6. (a) Proposed configuration for loading meander SW-TLs. (b) Field distribution of coupled SW-TLs.

to C_1. By reducing the tagged metal area for this capacitor in Fig. 1(c) $(A_1)C_1$ is decreased, which is realized by employing SSP cells with smaller groove depth d. Fig. 5(b) plots the ohmic loss per $10\lambda_1$ (λ_1 is the wavelength in free space at 20 GHz) for two SW-TLs A and B as well as a microstrip TL and a CPW line. The four cases are on FR4 substrate layers with the thickness of 0.26 mm. SW-TL A has the following parameters: $p = 4$ mm, $w = 2$ mm, $d = 0.9$ mm, and $g = 0.25p$. For SW-TL B, w and d are increased to 6 and 5 mm, respectively. The geometrical parameters of two SW-TLs are tabulated in Table II. The decay constant is calculated from the proposed circuit model by finding the imaginary part of

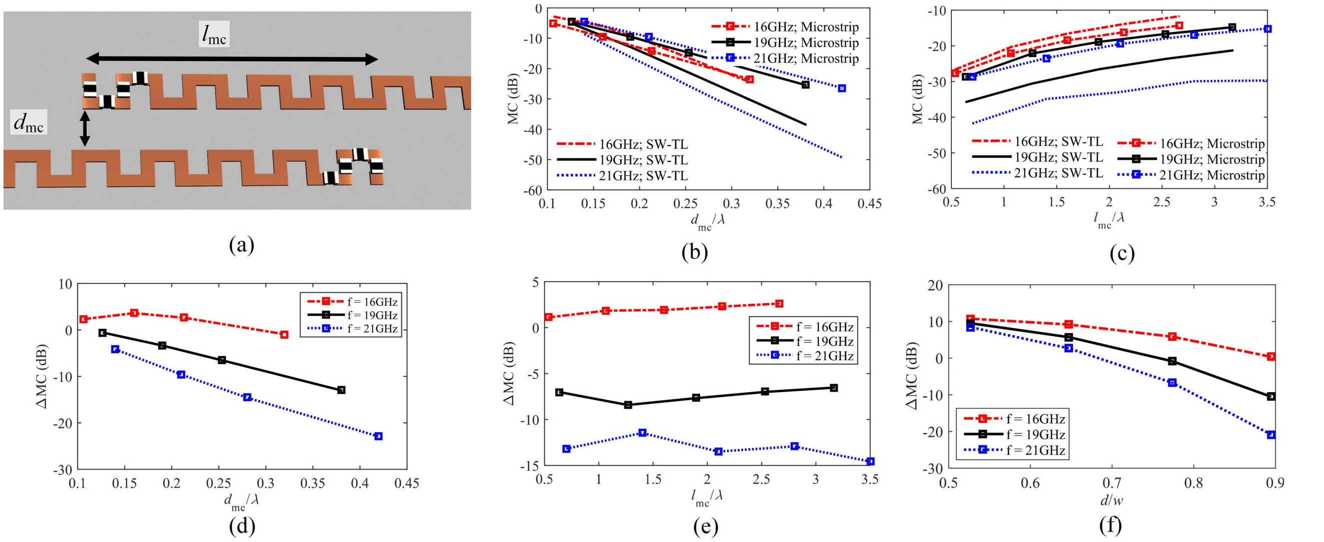

Fig. 7. MC calculation setup. (a) MC calculation setup. Comparison between meander SW-TLs and microstrip TLs at three frequencies of 16, 19, and 21 GHz for (b) varying coupling gap and (c) coupled line length. Difference between MC of SW-TLs and microstrip TLs for (d) varying coupling gap and (e) coupled line length. (f) Effect of groove depth of SSP cells on the MC between SW-TLs.

TABLE II
GEOMETRICAL PROPERTIES OF SW-TL A AND B

	p (mm)	w (mm)	d (mm)	a (mm)
SW-TL A	4	2	0.95	1
SW-TL B	4	6	5	1

the propagation constant in the periodic structure. The ohmic loss modeling is verified by the results from full-wave analysis by CST Microwave Studio in Fig. 5(b) and good agreement between them is observed for both SW-TLs.

SW-TL A achieves a much lower loss in comparison with the two conventional TLs on the same substrate over a wide frequency range from 5 to 26 GHz. These results show that by tuning the geometrical parameters of the SW-TL, both the low loss and lossy TLs can be designed. The ohmic loss calculation for the SW-TL is experimentally evaluated. To exclude the losses caused by the connectors and the mode converter from the measured results, two prototypes of SW-TL A with total lengths of 10 and 21 cm were fabricated. The insertion loss of the longer SW-TL by that of the shorter one is offset to get the ohmic loss over 11 cm of the TL. The measured scattering parameters are compared with the simulation in Fig. 5(c). The experimental results are in good agreement with simulation and confirm the proposed ohmic loss modeling method.

IV. MUTUAL COUPLING BETWEEN SW-TLS

The MC is an important feature of TLs and is defined as the coupling between the adjacent lines. In this section, the MC between the meander SW-TLs is studied and compared with MC between the microstrip TLs.

A. Broadband Loading for Meander SW-TL

To properly assess the MC between the matched SW-TLs, broadband loadings are required to be designed for the TLs. For this purpose, loading resistors can be placed through the current path of the SW-TLs. A design method of resistive loading for H-shaped SW-TLs is proposed in [35]. Here, a similar approach is applied; the TL is cut and then resistive loads bridge the gaps. Fig. 6(a) depicts a truncated SW-TL, which is loaded by four resistors: R_1, R_2, R_3, and R_4.

The broadband loading for an SW-TL composed of the SSP cells with the following parameters is designed: $p = 2$ mm, $w = 1.9$ mm, $d = 0.85w$, and $g = 0.25p$. The supporting substrate is Rogers 4003 with the thickness of 0.8 mm. The designed loaded SW-TL is used to study the MC here.

To achieve a broadband loading, the resistors are optimized. While using full-wave analysis is time consuming, the proposed equivalent circuit model in Section II eases the process significantly and can be integrated into the equivalent circuit-based models of systems. The loaded cells are included in the circuit model shown in Fig. 1(b) by additional resistors in series with the corresponding inductors. The following values are optimized for the resistors: $R_1 = 10\ \Omega$, $R_2 = 20\ \Omega$, $R_3 = 36\ \Omega$, and $R_4 = 56\ \Omega$. The resistors gradually increase from 10 to 56 Ω to provide a smooth transition from unloaded to loaded SSP cells.

B. MC Between Meander SW-TLs

The electric field distribution near two coupled SW-TLs is plotted in Fig. 6(b). The high field confinement of SSP modes causes low mutual effect between the two SW-TLs in comparison with that between guiding mode-based TLs. Fig. 7(a) shows two closely located SW-TL sections with the coupled line length of l_{mc} and coupling gap of d_{mc}. Fig. 7(b) and (c) compares the MC of the SW-TLs and microstrip TLs for varying d_{mc} and l_{mc}, respectively. For the results as shown in Fig. 7(b), l_{mc} is 50 mm and for those in Fig. 7(c), d_{mc} is 4 mm. The supporting substrate is Rogers 4003C with the thickness of 0.8 mm. The strip width of the microstrip TL is set as 1.9 mm to achieve the

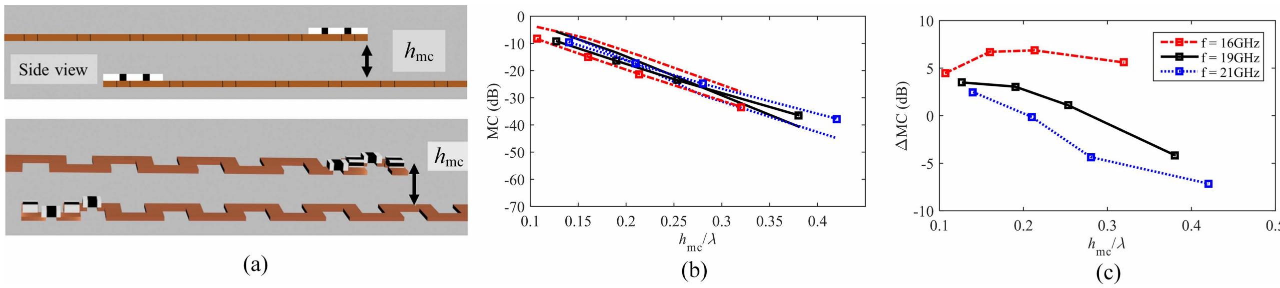

Fig. 8. (a) Setup for studying the MC between vertically separated SW-TLs. Comparison of the simulated MC between meander SW-TLs and microstrip TLs for varying vertical separations at three frequencies of 16, 19, and 21 GHz. (b) MC value and (c) difference between MC values.

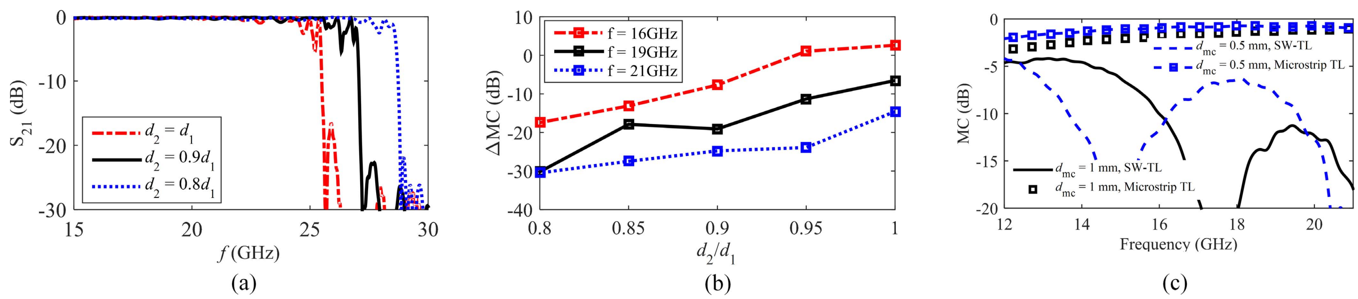

Fig. 9. (a) Transmission results from SW-TLs with different groove depths. (b) Effect of the groove depth ratio of two SW-TLs on their MC. Abscissa is the ratio between the groove depths of two coupled SW-TLs (d_2/d_1). Vertical axis is the MC difference between microstrip TLs and SW-TLs. Coupling gap and coupled line length are 4 and 50 mm, respectively. (c) MC of closely located SW-TLs and microstrip TLs.

50-Ω characteristic impedance. As seen, increasing d_{mc} and decreasing l_{mc} lower the MC. Moreover, at higher frequencies, where the field confinement of SSP modes is stronger, the MC between SW-TLs is lower.

Fig. 7(d) and (e) depicts the MC difference (ΔMC) between the microstrip TLs ($\mathrm{MC}_{\mathrm{microstrip}}$) and SW-TLs ($\mathrm{MC}_{\text{SW-TL}}$)

$$\Delta\mathrm{MC} = \mathrm{MC}_{\text{SW-TL}} - \mathrm{MC}_{\mathrm{microstrip}}. \tag{2}$$

With these results, SW-TLs show slightly higher coupling in comparison with the microstrip TLs at 16 GHz; however, as the frequency increases, the MC between SW-TLs decreases. The MC is directly proportional to the field confinement of SSP modes, which is directly related to their momentum: the SSP modes with larger momentum feature higher field confinement. Here, as the frequency increases the momentum increases, which results in lower the MC between SW-TLs and at 21 GHz, the MC between SW-TLs reaches the minimum.

Moreover, Fig. 7(b) indicates that the MC for SW-TLs more strongly depends on the coupling gap in comparison with that for the microstrip TLs. As the coupling gap increases, the MC between SW-TLs significantly decreases, and according to the results in Fig. 7(d), ΔMC is lower than -20 dB for $d_{\mathrm{mc}} = 0.4\lambda$ at 21 GHz. This is due to the higher field amplitude of the SSP modes near the meander structure, where the mutual effect of the SW-TLs is stronger.

Similar to the ohmic loss, the MC between the meander SW-TLs can be minimized by adjusting the geometrical parameters of SSP cells. Adjustability of the coupling enables design of highly isolated as well as highly coupled TLs based on the meander cells for different applications.

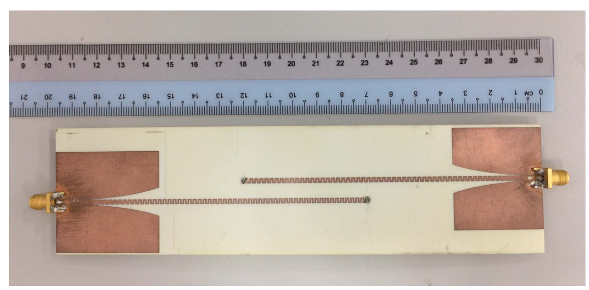

Fig. 10. Fabricated prototype of coupled SW-TLs.

Fig. 7(f) compares the MC between the SW-TLs for varying groove depths (the abscissa is d and is scaled to the SSP width). This figure plots the ΔMC between the microstrip TLs and the SW-TLs. The other parameters are set as $p = 2$ mm, $w = 1.9$ mm, and $g = 0.25p$. The coupling gap and the coupled line length are set as $d_{\mathrm{mc}} = 4$ mm and $l_{\mathrm{mc}} = 50$ mm. Decreasing d decreases the momentum of the SSP modes and consequently increases the coupling, as seen in Fig. 7(f). With the results, by choosing $d = 0.53w$, the coupling between the SW-TLs is about 10 dB higher than the MC between the microstrip TLs.

The MC between the vertically separated SW-TLs as depicted in Fig. 8(a) is studied in Fig. 8(b) and (c). The results are plotted for the coupled line length (l_{mc}) of 50 mm and variable vertical separation (h_{mc}). As the benchmark, the MC between the vertically separated microstrip TLs is compared with the results. For the microstrip TLs, the energy is mainly distributed in the dielectric substrate, and consequently, the MC for this configuration is very low. As seen, at lower

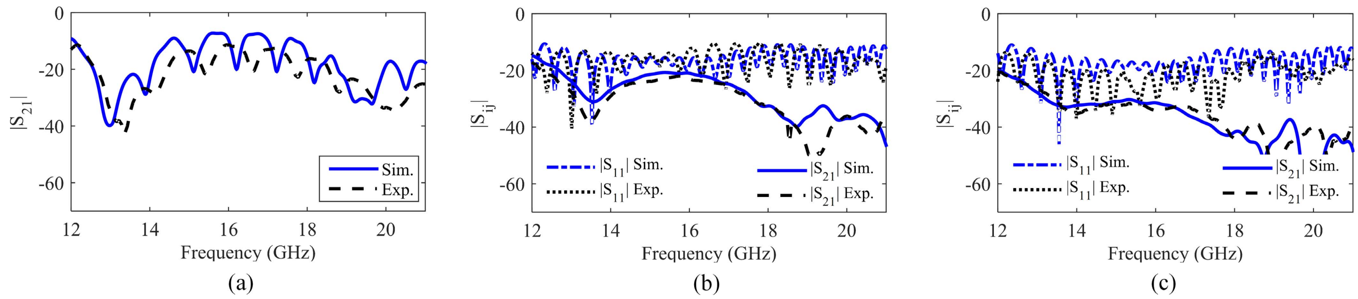

Fig. 11. Experimental evaluation of the scattering results of coupled SW-TLs for three cases. (a) SW-TLs (open ended) with the coupling gap of 2 mm. (b) SW-TLs (loaded) with the coupling gap of 4 mm. (c) SW-TLs (loaded) with the coupling gap of 6 mm.

frequencies with weak field confinement of the SSP modes, the SW-TLs show higher MC in comparison with that of microstrip TLs; however, as the frequency increases, the MC between the SW-TLs decreases and at 21 GHz, the ΔMC reaches -7 dB.

The results in Fig. 8(c) indicate that the MC dependence on the TL separation h_{mc} between the SW-TLs is much higher than that between the microstrip TLs because of the strong field confinement of the SSP modes. In other words, the majority of the energy distributes close to the SSP cells and it decays in space with a higher rate in comparison with microstrip TLs.

C. Suppression of MC Between Meander SW-TLs

Cumulative coupling along two adjacent TLs is caused by matching of the phase distribution of the modes over the two lines. In contrast, changing the phase distribution of one line could significantly decrease the MC. Considering two SW-TLs by the change of the SSP cells of one line, the two lines no longer support identical SSP modes. Different SSP modes have different dispersion characteristics and different phase distributions, and consequently, nonidentical SW-TLs feature lower MC in comparison with the identical SW-TLs. This subsection studies the MC between two SW-TLs (SW-TL I and SW-TL II) with different groove depths. SW-TL I composed of SSP cells with the following parameters: $p_1 = 2$ mm, $w_1 = 1.9$ mm, $d_1 = 0.85w_1$, and $g_1 = 0.25p_1$, while SW-TL II is composed of similar meander cells but with different groove depth: $p_2 = p_1$, $w_2 = w_1$, $g_2 = g_1$, and $d_2 \neq d_1$.

The change of the groove depth affects the cutoff frequency of the SW-TLs. Fig. 9(a) depicts the transmission spectrum of the SW-TL II for varying d_2. As seen at $d_2 = d_1$, the cutoff frequency is 25 GHz. By changing d_2 to 0.9 d_1 and 0.8 d_1, the cutoff frequency increases to 27 and 29 GHz, respectively; however, all the three cases operate efficiently within the frequency range from 15 to 25 GHz.

Fig. 9(b) studies the MC between SW-TLs I and II for varying d_2 against frequencies for $d_{\mathrm{mc}} = 4$ mm and $l_{\mathrm{mc}} = 50$ mm. The abscissa is the groove depth ratio between SW-TL I and SW-TL II (d_2/d_1). The vertical axis is ΔMC defined in (2). As seen, by decreasing d_2 from d_1 to 0.8 d_1, the MC significantly decreases, where ΔMC hits -30 dB at 21 GHz. The MC reduction between the SW-TLs with different SSP cells is due to the different supporting modes of the two TLs, which suppresses their coupling effects. This result is far below the realized MC between the single-layered SSP-based TLs with coplanar face-to-face configurations reported in [35]. Moreover, these results along with the high ΔMC of 10 dB achieved in Fig. 7(f) demonstrate the dynamic range of 40 dB for the control of the MC of meander SW-TLs. This MC controlling feature is a unique advantage, which enables the further changes of the MC between the SW-TLs within a fixed configuration.

The proposed MC suppression method is also effective for very closely located SW-TLs. Fig. 9(c) compares the MC of SW-TLs and microstrip TLs with a coupling gap of $d_{\mathrm{mc}} = 1$ and 0.5 mm. The MC between the microstrip lines exceeds -1 dB. This high coupling is expectable of a very small spacing of less than half of the strip width. The SW-TL, on the other hand, shows significantly better isolation, especially at higher frequencies.

For experimental verification purposes, closely located SW-TLs I and II are fabricated for three line separations of $d_{\mathrm{mc}} = 2$, 4, and 6 mm. One of the fabricated prototypes is shown in Fig. 10. The groove depth ratio is 0.8 and the coupled line length is $l_{\mathrm{mc}} = 50$ mm. Fig. 11(a) displays the MC between two SW-TLs with $d_{\mathrm{mc}} = 2$ mm when the ends are open. Fig. 11(b) and (c) plots the scattering parameter results from the loaded SW-TLs with $d_{\mathrm{mc}} = 4$ and 6 mm, respectively. As seen, the experiment well matches the simulation and shows the accuracy of the MC calculation setup.

V. Conclusion

This paper has proposed a geometric-based equivalent circuit model for the meander SSP cells. The ohmic loss caused by meander SSP cells has been modeled by adding parallel conductance to the capacitor, where the modeling has applied to minimize the ohmic loss of meander SW-TLs. Moreover, the MC between meander SW-TLs has been compared with conventional microstrip TLs. It has been shown that meander SSP cells have provided the extra degrees of freedom to adjust the coupling between the SW-TLs at the desired frequency, and consequently, enabled the design of highly isolated as well as highly coupled TLs. The equivalent model and the simulation results have been verified experimentally by measuring the transmission, return loss, ohmic loss, and MC of fabricated SW-TLs.

REFERENCES

[1] J. B. Pendry, L. Martín-Moreno, and F. J. Garcia-Vidal, "Mimicking surface plasmons with structured surfaces," *Science*, vol. 305, pp. 847–848, Aug. 2004.

[2] F. F. Qin, J. J. Xiao, Z. Z. Liu, and Q. Zhang, "Multiple fano-like transmission mediated by multimode interferences in spoof surface plasmon cavity-waveguide coupling system," *IEEE Trans. Microw. Theory Techn.*, vol. 64, no. 4, pp. 1186–1194, Apr. 2016.

[3] J. R. Middendorf, J. S. Cetnar, J. Owsley, and E. R. Brown, "High fill-factor substrate-based wire-grid polarizers with high extinction ratios," *IEEE Trans. THz Sci. Technol.*, vol. 4, no. 3, pp. 376–382, May 2014.

[4] M. Aghadjani and P. Mazumder, "THz polarizer controller based on cylindrical spoof surface plasmon polariton (C-SSPP)," *IEEE Trans. THz Sci. Technol.*, vol. 5, no. 4, pp. 556–563, Jul. 2015.

[5] X. Shen, T. J. Cui, D. F. Martin-Cano, and J. Garcia-Vidal, "Conformal surface plasmons propagating on ultrathin and flexible films," *Proc. Nat. Acad. Sci. USA*, vol. 110, no. 1, pp. 40–45, 2013.

[6] H. Shi, X. Wei, Z. Zhao, X. Dong, Y. Lu, and C. Du, "A new surface wave antenna-based spoof surface plasmon mechanism," *Microw. Opt. Technol. Lett.*, vol. 52, no. 10, pp. 2179–2183, 2010.

[7] J. J. Xu, H. C. Zhang, Q. Zhang, and T. J. Cui, "Efficient conversion of surface-plasmon-like modes to spatial radiated modes," *Appl. Phys. Lett.*, vol. 106, no. 2, 2015, Art. no. 021102.

[8] H. Yi, S.-W. Qu, and X. Bai, "Antenna array excited by spoof planar plasmonic waveguide," *IEEE Antennas Wireless Propag. Lett.*, vol. 13, pp. 1227–1230, 2014.

[9] O. Quevedo-Teruel, "Controlled radiation from dielectric slabs over spoof surface plasmon waveguides," *Prog. Electromagn. Res.*, vol. 140, no. 4, pp. 169–179, 2013.

[10] J. J. Wu *et al.*, "High-directivity radiation based on the leaky mode of spoof surface plasmon polaritons," *IET Microw., Antennas Propag.*, vol. 8, no. 13, pp. 1075–1079, 2014.

[11] A. Kianinejad, Z. N. Chen, L. Zhang, W. Liu, and C.-W. Qiu, "Spoof plasmon-based slow-wave excitation of dielectric resonator antennas," *IEEE Trans. Antennas Propag.*, vol. 64, no. 6, pp. 2094–2099, Jun. 2016.

[12] A. Kianinejad, Z. N. Chen, and C.-W. Qiu, "A single-layered spoof-plasmon-mode leaky wave antenna with consistent gain," *IEEE Trans. Antennas Propag.*, vol. 65, no. 2, pp. 681–687, Feb. 2017.

[13] A. Kianinejad, Z. N. Chen, and C.-W. Qiu, "Spoof surface plasmon-based leaky wave antennas," in *Proc. Asia–Pacific Microw. Conf. (APMC)*, New Delhi, India, Dec. 2016, pp. 1–3.

[14] G. Goubau, "Open wire lines," *IRE Trans. Microw. Theory Techn.*, vol. 4, no. 4, pp. 197–200, 1956.

[15] A. Treizebre, T. Akalin, and B. Bocquet, "Planar excitation of Goubau transmission lines for THz BioMEMS," *IEEE Microw. Wireless Compon. Lett.*, vol. 15, no. 12, pp. 886–888, Dec. 2005.

[16] T. Akalin, E. Peytavit, and J.-F. Lampin, "THz long range plasmonic waveguide in membrane topology," in *Proc. 33rd Int. Conf. Infr., Millim. Terahertz Waves (IRMMW-THz)*, Sep. 2008, pp. 1–2.

[17] T. Akalin and W. Padilla, "Plasmonic waveguides and metamaterial components at terahertz frequencies," in *Proc. Asia–Pacific Microw. Conf.*, Singapore, Dec. 2009, pp. 2444–2446.

[18] H. F. Ma, X. Shen, Q. Cheng, W. X. Jiang, and T. J. Cui, "Broadband and high-efficiency conversion from guided waves to spoof surface plasmon polaritons," *Laser Photon. Rev.*, vol. 8, no. 1, pp. 146–151, 2014.

[19] A. Kianinejad, Z. N. Chen, and C.-W. Qiu, "Design and modeling of spoof surface plasmon modes-based microwave slow-wave transmission line," *IEEE Trans. Microw. Theory Techn.*, vol. 63, no. 6, pp. 1817–1825, Jun. 2015.

[20] X. Gao *et al.*, "Ultrathin dual-band surface plasmonic polariton waveguide and frequency splitter in microwave frequencies," *Appl. Phys. Lett.*, vol. 102, no. 15, 2013, Art. no. 151912.

[21] X. Gao, L. Zhou, Z. Liao, H. F. Ma, and T. J. Cui, "An ultra-wideband surface plasmonic filter in microwave frequency," *Appl. Phys. Lett.*, vol. 104, no. 19, 2014, Art. no. 191603.

[22] J. Y. Yin, J. Ren, H. C. Zhang, Q. Zhang, and T. J. Cui, "Capacitive-coupled series spoof surface plasmon polaritons," *Sci. Rep.*, vol. 6, Apr. 2016, Art. no. 24605.

[23] B. Xu, Z. Li, L. Liu, J. Xu, C. Chen, and C. Gu, "Bandwidth tunable microstrip band-stop filters based on localized spoof surface plasmons," *J. Opt. Soc. Amer. B, Opt. Phys.*, vol. 33, no. 7, pp. 1388–1391, 2016.

[24] L. Liu *et al.*, "Dual-band trapping of spoof surface plasmon polaritons and negative group velocity realization through microstrip line with gradient holes," *Appl. Phys. Lett.*, vol. 107, no. 20, 2015, Art. no. 201602.

[25] J. Xu *et al.*, "Low-pass plasmonic filter and its miniaturization based on spoof surface plasmon polaritons," *Opt. Commun.*, vol. 372, pp. 155–159, Aug. 2016.

[26] Z. Li *et al.*, "Coplanar waveguide wideband band-stop filter based on localized spoof surface plasmons," *Appl. Opt.*, vol. 55, no. 36, pp. 10323–10328, 2016.

[27] X. Liu, Y. Feng, K. Chen, B. Zhu, J. Zhao, and T. Jiang, "Planar surface plasmonic waveguide devices based on symmetric corrugated thin film structures," *Opt. Express*, vol. 22, no. 17, pp. 20107–20116, 2014.

[28] X. Liu, Y. Feng, B. Zhu, J. Zhao, and T. Jiang, "High-order modes of spoof surface plasmonic wave transmission on thin metal film structure," *Opt. Express*, vol. 21, no. 25, pp. 31155–31165, 2013.

[29] Y. Liang *et al.*, "On-chip sub-terahertz surface plasmon polariton transmission lines with mode converter in CMOS," *Sci. Rep.*, vol. 6, Jul. 2016, Art. no. 30063.

[30] H. C. Zhang, Q. Zhang, J. F. Liu, W. Tang, Y. Fan, and T. J. Cui, "Smaller-loss planar SPP transmission line than conventional microstrip in microwave frequencies," *Sci. Rep.*, vol. 6, Mar. 2016, Art. no. 23396.

[31] X. Liu, L. Zhu, Q. Wu, and Y. Feng, "Highly-confined and low-loss spoof surface plasmon polaritons structure with periodic loading of trapezoidal grooves," *AIP Adv.*, vol. 5, no. 7, 2015, Art. no. 077123.

[32] R. Sato, "A design method for meander-line networks using equivalent circuit transformations," *IEEE Trans. Microw. Theory Techn.*, vol. MTT-19, no. 5, pp. 431–442, May 1971.

[33] M.-A. Joyal, M. Riel, Y. Demers, and J.-J. Laurin, "A meander-line circular polarizer optimized for oblique incidence," *IEEE Trans. Antennas Propag.*, vol. 63, no. 12, pp. 5391–5398, Dec. 2015.

[34] A. Kianinejad, *Metamaterial Surface Plasmon-Based Transmission Lines and Antennas* (Springer Theses), 1st ed. Singapore: Springer, 2018.

[35] A. Kianinejad, Z. N. Chen, and C.-W. Qiu, "Low-loss spoof surface plasmon slow-wave transmission lines with compact transition and high isolation," *IEEE Trans. Microw. Theory Techn.*, vol. 64, no. 10, pp. 3078–3086, Oct. 2016.

[36] J. J. Wu *et al.*, "Reduction of wide-band crosstalk for guiding microwave in corrugated metal strip lines with subwavelength periodic hairpin slits," *IET Microw., Antennas Propag.*, vol. 6, no. 2, pp. 231–237, Jan. 2012.

[37] Y. Liang, H. Yu, H. C. Zhang, C. Yang, and T. J. Cui, "On-chip sub-terahertz surface plasmon polariton transmission lines in CMOS," *Sci. Rep.*, vol. 5, Oct. 2015, Art. no. 14853.

[38] Y. Liang, H. Yu, G. Feng, A. A. A. Apriyana, X. Fu, and T. J. Cui, "An energy-efficient and low-crosstalk sub-THz I/O by surface plasmonic polariton interconnect in CMOS," *IEEE Trans. Microw. Theory Techn.*, vol. 65, no. 8, pp. 2762–2774, Aug. 2017.

[39] H. C. Zhang, T. J. Cui, Q. Zhang, Y. Fan, and X. Fu, "Breaking the challenge of signal integrity using time-domain spoof surface plasmon polaritons," *ACS Photon.*, vol. 2, no. 9, pp. 1333–1340, 2015.

[40] Z. Piatek, B. Baron, T. Szczegielniak, D. Kusiak, and A. Pasierbek, "Self inductance of long conductor of rectangular cross section," *Przeglad Elektrotechniczny*, vol. 88, no. 8, pp. 323–326, 2012.

[41] D. M. Pozar, *Microwave Engineering*, 3rd ed. New York, NY, USA: Wiley, 2004.

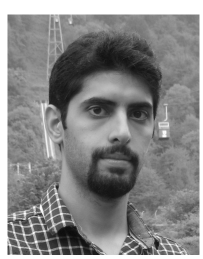

Amin Kianinejad (S'14–M'17) received the B.Sc. degree in electrical engineering from the Shiraz University of Technology, Shiraz, Iran, in 2008, the M.Sc. degree in electrical engineering from the Sharif University of Technology, Tehran, Iran, in 2010, and the Ph.D. degree in electrical engineering from the National University of Singapore (NUS), Singapore, in 2017.

He is currently a Research Fellow with the Department of Electrical and Computer Engineering with NUS, Singapore. His current research interests include microwave plasmonics, antennas, and metamaterials.

Dr. Kianinejad was a recipient of the Springer Thesis Award 2017, the Best Student Paper Award (Second Prize) in International Workshop on Antenna Technology 2017, and the Best Student Paper Competition Award 2016 from the IEEE Singapore MTT/AP Joint Chapter.

Zhi Ning Chen (M'99–SM'05–F'07) received the B.Eng., M.Eng., and Ph.D. degrees in electrical engineering from the Institute of Communications Engineering (ICE), China, and the Ph.D. degree from the University of Tsukuba, Tsukuba, Japan.

From 1988 to 1995, he was a Lecturer and an Associate Professor with ICE, as well as a Post-Doctoral Fellow and an Associate Professor with Southeast University, Nanjing, China. From 1995 to 1997, he was a Research Assistant with the City University of Hong Kong, Hong Kong and later become a Research Fellow. From 1999 to 2016, he was a Principal Scientist with the Institute for Infocomm Research (I2R), Singapore, where he was the Head of the RF and Optical Department and the Technical Advisor. In 2001 and 2004, he visited the University of Tsukuba under the Japan Society for the Promotion of Science (JSPS) Fellowship Program (at a senior level). In 2004, he was an Academic Visitor with the IBM T. J. Watson Research Center, Yorktown Heights, NY, USA. In 2012, he joined the Department of Electrical and Computer Engineering, National University of Singapore, Singapore, as a tenured Full Professor, where he is currently a Program Director (Industry). In 2013, he visited the Laboratoire des SignauxetSystèmes, CNRS-Supelec, University Paris Sud, Gif-sur-Yvette, France, as a Senior DIGITEO Guest Scientist. He is currently holding concurrent guest professorships with Nanjing University, Nanjing, Tsinghua University, Beijing, China, Shanghai Jiaotong University, Shanghai, China, Tongji University, Shanghai, the University of Science and Technology of China, Hefei, China, Dalian Maritime University, Dalian, China, Chiba University, Chiba, Japan, National Taiwan University of Science and Technology, Taipei City, Taiwan, Beijing University of Posts and Telecommunications, Beijing, and Tohoku University, Sendai, Japan. He is also a Changjiang Chair Professor with Southeast University, a Outstanding Visiting Professor with Fudan University, Shanghai, a Ziqiang Professor with Shanghai University, Shanghai, and an Adjunct Professor with the City University of Hong Kong. He is also serving as a member of the State Key Laboratory of Millimeter-waves, Southeast University and the City University of Hong Kong. He has authored or co-authored more than 580 academic papers and the books *Broadband Planar Antennas* (Wiley, 2005), *UWB Wireless Communication* (Wiley, 2006), *Antennas for Portable Devices* (Wiley, 2007), *Antennas for Base Stations in Wireless Communications* (McGraw-Hill, 2009), and *Handbook of Antenna Technologies* with 76 chapters (by Springer References in 2016 as an Editor-in-Chief). He has also contributed chapters to *UWB Antennas and Propagation for Communications, Radar, and Imaging* (Wiley, 2006), *Antenna Engineering Handbook* (McGraw-Hill, 2007), *Microstrip and Printed Antennas* (Wiley, 2010), and *Electromagnetics of Body Area Networks* (Wiley, 2016). He holds 28 granted/filed patents with 35 licensed deals with industry. His current research interests include electromagnetic engineering and antennas/sensors for communication, radar, imaging and sensing systems.

Dr. Chen is the founding General Chair of the International Workshop on Antenna Technology (iWAT) in 2005, the International Symposium on InfoComm and Mechatronics Technology in Biomedical and Healthcare Application (IS 3Tin3A) in 2010, the International Microwave Forum in 2010, and the Asia–Pacific Conference on Antennas and Propagation in 2012. He also involved in many international events as a General Chair, Chair, and member of Technical Program Committees and International Advisory Committees. He was a recipient of the JSPS Fellowship to conduct his research at the University of Tsukuba, in 1997, the International Symposium on Antennas and Propagation Best Paper Award in 2010, the CST University Publication Award in 2008 and 2015, the ASEAN Outstanding Engineering Achievement Award in 2013, the Institution of Engineers Singapore Prestigious Engineering Achievement Award in 2006, 2013, and 2014, the I2R Quarterly Best Paper Award in 2004, the IEEE iWAT 2005 Best Poster Award, several Technology Achievement Awards of China from 1990 to 1997, as well as more than 19 academic awards by the students he supervised. He has been serving the IEEE Council on RFID as a Vice President and a Distinguished Lecturer since 2015. He was an Associate Editor of the IEEE TRANSACTION ON ANTENNAS AND PROPAGATION and a Distinguished Lecturer of the IEEE Antennas and Propagation Society.

Cheng-Wei Qiu (S'03–M'08) received the B.Eng. and Ph.D. degrees in 2003 and 2007, respectively.

He was a Post-Doctoral Fellow with the Physics Department, MIT, in 2009. Since 2009, he has been an Assistant Professor with the National University of Singapore (NUS), Singapore, and an Associate Professor with tenure in 2017. In 2018, he became the Dean's Chair with the Faculty of Engineering, NUS. His current research interests include electromagnetic theory and applications, metasurfaces, and structured light for beam manipulation and nanoparticle manipulation.

Dr. Qiu served as the General Chair, the Symposium Chair, and the TPC Chair in various international conferences. He was a recipient of the SUMMA Graduate Fellowship in Advanced Electromagnetics in 2005, the IEEE AP-S Graduate Research Award in 2006, the URSI Young Scientist Award in 2008, the NUS Young Investigator Award in 2011, the MIT TR35 at Asia Award in 2012, the Young Scientist Award of the Singapore National Academy of Science in 2013, the Faculty Young Research Award of NUS 2013, the OSA Young Investigator Award in 2017, the Young Engineering Research Award in 2018 of NUS, and the SPIE Rising Researcher Award in 2018.